Article:
Liu, Y., Huang, S.-S. and Burgess, I. (2022) Ductile connection to improve the fire performance of bare-steel and composite frames. Journal of Structural Fire Engineering, 13 (2). pp. 249-266. ISSN: 2040-2317

https://doi.org/10.1108/jsfe-06-2021-0041

Ductile Connection to Improve the Fire Performance of Bare-steel and Composite Frames

ABSTRACT

In order to improve the robustness of bare-steel and composite structures in fire, a novel axially and rotationally ductile connection has been proposed. The component-based models of the bare-steel ductile connection and composite ductile connection have been proposed and incorporated into the software Vulcan to facilitate global frame analysis for performance-based structural fire engineering design. These component-based models are validated against detailed Abaqus FE models and experiments. A series of 2-D bare-steel frame models and 3-D composite frame models with ductile connections, idealised rigid and pinned connections, have been created using Vulcan to compare the fire performance of ductile connection with other connection types in bare-steel and composite structures. The comparison results show that the proposed ductile connection can provide excellent ductility to accommodate the axial deformation of connected beam under fire conditions, thus reducing the axial forces generated in the connection and potentially preventing the premature brittle failure of the connection.

Keywords: Fire; component-based model; ductility; steel connection; composite connection

Notation list

V_{Rd}	The shear capacity of the semi-cylindrical section
A_v	The cross-sectional area of the semi-cylindrical section
$\Delta_{low-temp}$	Axial ductility demand of steel beam in the early heating stage
$\Delta_{high-temp,\max}$	Axial ductility demand of steel beam at the connection top surface (high temperature)
$\Delta_{high-temp}$	Axial ductility demand of steel beam at the connection bottom surface (high temperature)
l	The length of the steel/composite beam

α Thermal expansion coefficient of steel

T Beam temperature

h The height of the steel beam section

δ The mid-span deflection of the steel beam

Δ_r Axial ductility demand of the composite beam at the rebar level

Δ_{cts} Axial ductility demand of the composite beam at the connection top surface

Δ_{cbs} Axial ductility demand of the composite beam at the connection bottom surface

Δ_{bbf} Axial ductility demand of the composite beam at the beam bottom flange

θ_{total} Total rotation of the composite beam at beam end

δ_{total} Total deflection of the composite beam, $\delta_{total} = \delta_{external-load} + \delta_{thermal-bowing}$

h_1 Slab depth

h_2 Steel beam depth

H_{con} Connection depth

h_c The vertical distance from the top surface of the slab to the neutral axis

h_r The vertical distance from the top surface of the slab to the longitudinal rebar

1 INTRODUCTION

Connection failures which occurred in the collapse of the World Trade Centre buildings (McAllister and Corley, 2002) and the Cardington full-scale fire tests (Lennon and Moore, 2003) indicate that standard connections are potentially the weakest parts of a steel-framed or composite structure. The failure of connections may lead to the detachment of connected beams, collapse of floor, spread of fire into other compartments, buckling of columns and even the final progressive collapse of the entire building.

Conventional commonly-used connection types lack axial and rotational deformability to accommodate the large deformation that a connected beam would experience in a fire accident. In order to improve the fire performance of connections, a novel connection with excellent axial and rotational ductility has been proposed by the authors (Liu et al., 2019a, 2019b, 2020a, 2020b, 2020c, 2021a, 2021b, 2021c).

During a fire event, connections undergo different combinations of axial forces, shear forces and bending moments, transferred from the connected structural members at different stages. It is difficult to reproduce such complex loading conditions in experiments, other than in full-scale fire tests. Therefore, numerical modelling is a more feasible way to investigate connection behaviour, considering the effects of degraded material properties, thermal expansion, and combinations of forces in fire conditions. Compared with detailed finite element modelling, the component-based method is a practical compromise between accuracy and computational cost. In the component-based method, the connection is considered as an assembly of basic components and each component is represented by a non-linear spring. The component-based modelling strategies and component models of traditional steelwork connections, have been proposed as a result of studies (Leston-Jones, 1997, Spyrou, 2002, Block, 2006, Sarraj, 2007, Sarraj et al., 2007, Yu et al., 2009a, 2009b, Dong, 2016, Hu et al., 2009, Taib and Burgess, 2013) over many years by the structural fire engineering research group at the University of Sheffield. Leston-Jones (1997) proposed a component-based model for the flush end-plate connection, which includes components representing bolts in tension, endplate in bending, column flange in bending and column web in compression. Block (2006) proposed a component-based model for end-plate connection, which derives from a T-stub analytical model developed by Spyrou (2002) to represent tension bolt rows and a simplified analytical model of the column web in compression to represent the compression zone of the connection. Based on a series of finite element parametric studies, equations were derived to describe the bearing and shearing behaviour of fin-plate connection (Sarraj, 2007, Sarraj et al., 2007). Yu (2009a) developed a yield-line based model for end-plate connections and a component-based model for web-cleat connections (Yu et al., 2009b). Hu (2009) developed a flexible end-plate connection model and Taib (Taib and Burgess, 2013) developed a fin-plate connection model. Dong (2016) proposed a used-defined connection model, a flush end-plate connection

model and a reverse-channel connection model, and incorporated them all into the software Vulcan (Najjar and Burgess, 1996, Huang et al., 1999, Cai et al., 2003, Huang et al., 2003a, 2003b, 2009), which is a high-temperature frame analysis software developed by the Structural Fire Engineering Research Group at the University of Sheffield. The component-based models of the novel ductile connection have been developed by the authors (Liu et al., 2020a, 2021a) in the context of steel-framed and composite buildings, and have been incorporated into Vulcan to carry out global frame analysis.

Compared with bare-steel structures, composite construction allows the use of smaller steel sections, and therefore has higher structural efficiency and lower cost. The structural behaviour of connections in composite frames is quite different from that in bare-steel frames due to the composite slab, which can provide thermal insulation to the top part of the connection, reducing its temperature and enhancing its fire resistance. In addition, the composite slab restrains the thermal expansion of the steel beam, leading to the thermal bowing of flooring system, which also affects the connection behaviour. AI-Jabri (1999) conducted a series of high-temperature tests on flexible end-plate composite connections and proposed a component-based model to predict the response of the composite end-plate connections. Li et al. (2012) carried out three tests on flush end-plate composite joints. Based on the experimental results, they proposed a simplified method to calculate the non-linear characteristics of composite connection in the analysis of beam catenary action at elevated temperatures. Fischer and Varma (2017) built 3-D FE models of composite beams with simple connections to investigate the effect of connection type and slab reinforcement type on the performance of composite beams in fire. Up to now, research on the structural performance of composite connections is still very limited.

In this paper, the ductility demands of bare-steel and composite beams in fire, the design of the novel ductile connection, and the component-based models of bare-steel and composite ductile connection are summarised. The bare-steel component-based model has first been validated against experiments at both ambient and elevated temperatures. The 2-D sub-frame models of the ductile connection, bare-steel and composite, are then used to further verify the component-based models, and to assess if they are correctly

incorporated into Vulcan, by comparing the Vulcan results against detailed finite element modelling using Abaqus. Finally, the structural performance of the ductile connection in steel and composite structures is compared with those of conventional types of connections.

2 THE PROPOSED DUCTILE CONNECTION

2.1 Design of the ductile connection

The proposed ductile connection includes two identical parts, each of which may be characterised as a fin-plate which is bolted to the beam web, a face-plate which is bolted to either the column flange or web, and a semi-cylindrical section between these two parts, as shown in Figure 1.

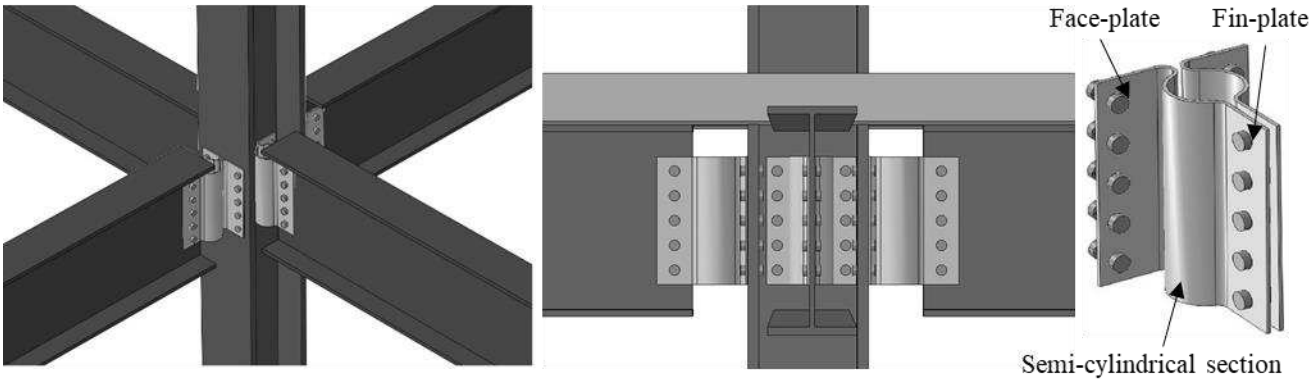

Figure 1. The proposed novel connection

The ductile connection should be adequate for ambient-temperature ultimate limit state conditions, therefore, the resistance of the ductile connection should be checked according to the Eurocode (CEN, 2005) including bolt shear, bolt bearing, shear and bearing of the fin-plate, shear and bearing of the bolt group and shear of the end-plate. The basic part of this ductile connection can be manufactured by simply bending a steel plate. The fin-plate part of the ductile connection can be directly designed according to the Eurocode. The dimensions of the face-plate part of the ductile connection can be determined using the Eurocode rules for the end-plate connection. The ambient-temperature shear capacity of the semi-cylindrical section is determined using Equation (1). The high-temperature shear capacity of the semi-cylindrical section does not need to be checked, since shear failure is very unlikely to occur in the semi-

cylindrical section at high temperatures, given that detailed Abaqus modelling (Liu et al., 2019b, 2021a) shows little vertical deflection of the ductile connection at elevated temperatures. Since the ductile connection can be regarded as a simple connection, the beam with ductile connections at both ends can be designed as a simply supported beam.

$$V_{Rd} = A_v f_y / (\sqrt{3}\gamma_{M0}) \tag{1}$$

The semi-cylindrical section is the most critical component, since it provides required additional push-pull ductility by allowing the fin-plate to move towards and away from the face-plate. Therefore, the radius of the semi-cylindrical section is the most important parameter for the entire ductile connection and should be determined carefully. The radius should not be too small, otherwise the ductility of the connection will be reduced and the axial force generated in the adjacent structural components will be increased. The radius is, therefore, determined according to the ductility demand of the connected beam during a fire event. This will be introduced in detail in Section 2.2.

2.2 Ductility demands of steel and composite beams in fire

In bare-steel frames, during the initial heating stage of a fire (usually below 600°C), the connection should be able to accommodate the axial displacement $\Delta_{low-temp}$, caused by the beam thermal expansion, beam end rotation and beam shortening due to deflection, as shown in Figure 2 (a). When the high temperature range is reached, the steel beam usually enters the catenary action stage. In order to prevent fracture at the top of the connection and to avoid hard contact between the beam bottom flange and column face, the connection should be able to accommodate the displacements $\Delta_{high-temp,\max}$ in tension and $\Delta_{high-temp}$ in compression, as shown in Figure 2 (a). In composite frames, there are four key positions where the axial displacement of the beam end needs to be taken into consideration, including the rebar level, the top surface of the connection, the bottom surface of the connection, and the bottom flange of the beam, as shown in Figure 2 (b). It should be noted that the total deflection δ_{total} of the composite beam includes the deflection due to thermal bowing and the deflection caused by external loads. Equations (2) - (8) proposed by the authors

(Liu et al., 2020a, 2021a) can be used to calculate the ductility demands of steel beam (Equations (2) - (4)) and composite beam (Equations (5) - (8)) in fire. As mentioned previously, the radius of the semi-cylindrical section should be determined according to the ductility demands of the connected beam in fire. Therefore, the cylindrical section radius of the bare-steel ductile connection should be larger than the maximum value of $\Delta_{low-temp}$, $\Delta_{high-temp}$ and $\Delta_{high-temp}$, and the cylindrical section radius of the composite ductile connection should be larger than the maximum value of Δ_{r}, Δ_{cts}, Δ_{cbs} and Δ_{bbf}. However, a semi-cylindrical section with too large a radius may hinder the installation of bolts. Therefore, further investigation is needed to provide a criterion for determining the upper limit of the radius. The criterion could be stated by considering the geometric relationship between the bolt position, the bolt size and the size of the semi-cylindrical section.

$$\Delta_{low-temp}=\frac{1}{2}(\alpha lT+h\theta)-\frac{4}{3}\delta^{2}/l \tag{2}$$

$$\Delta_{high-temp}=\frac{4}{3}\delta_{\max}{}^{2}/l-\frac{1}{2}(\alpha lT+h\theta) \tag{3}$$

$$\Delta_{high-temp,\max}=\frac{4}{3}\delta_{\max}{}^{2}/l-\frac{1}{2}(\alpha lT-h\theta) \tag{4}$$

$$\Delta_{\mathrm{r}}=\frac{4}{3}\delta_{total}{}^{2}/l-\tan\left(\theta_{total}\right)\cdot\left(h_{r}-h_{c}\right) \tag{5}$$

$$\Delta_{cts}=\frac{4}{3}\delta_{total}{}^{2}/l-\tan\left(\theta_{total}\right)\cdot\left(h_{1}+\frac{h_{2}-H_{con}}{2}-h_{c}\right) \tag{6}$$

$$\Delta_{cbs}=\frac{4}{3}\delta_{total}{}^{2}/l-\tan\left(\theta_{total}\right)\cdot\left(h_{1}+\frac{h_{2}+H_{con}}{2}-h_{c}\right) \tag{7}$$

$$\Delta_{bbf}=\frac{4}{3}\delta_{total}{}^{2}/l-\tan\left(\theta_{total}\right)\cdot\left(h_{1}+h_{2}-h_{c}\right) \tag{8}$$

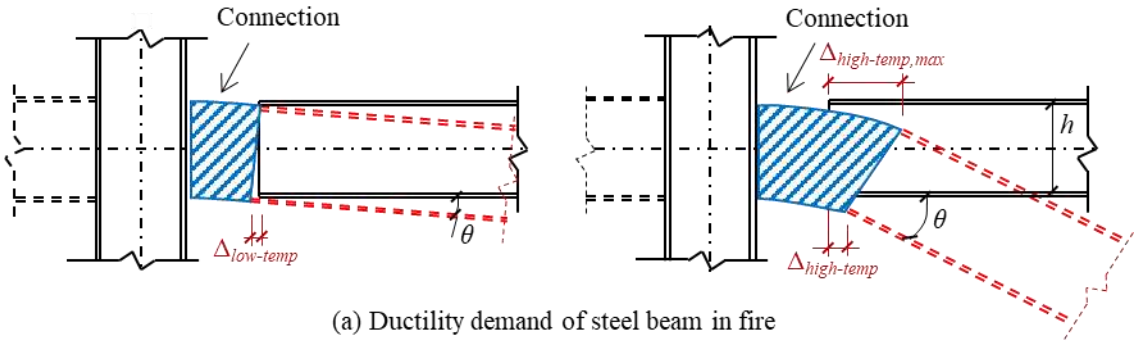

(a) Ductility demand of steel beam in fire

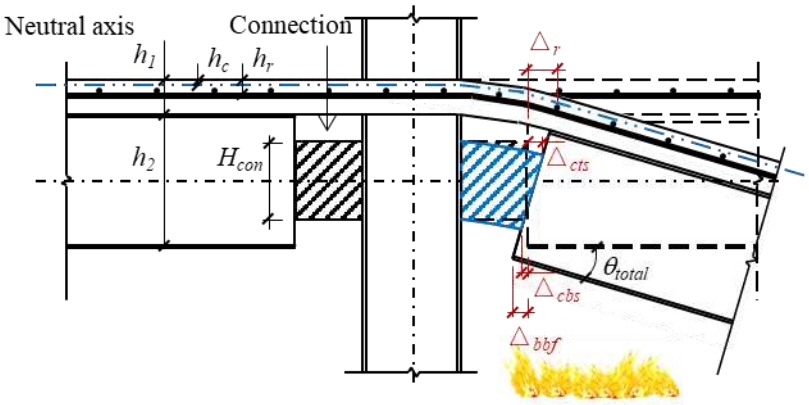

(b) Ductility demand of composite beam in fire

Figure 2. Ductility demands of steel and composite beams in fire

3 COMPONENT-BASED MODELS OF THE DUCTILE CONNECTION

Figure 3 (a) shows the schematic component-based model of the bare-steel ductile connection developed by the authors (Liu et al., 2020a). The two end nodes of the model are located at the intersection points between the reference axes of the connected beam and column. The component-based model is assumed to be rigid in the vertical direction, since the vertical shear behaviour representing the slip between the beam end and the column flange has not been considered. The basic components are listed in the figure, including fin-plate in bearing, beam web in bearing, bolt in shear, face-plate-semi-cylindrical component, bolt pull-out and column web in compression. The horizonal gap △ between the vertical rigid bar and column web represents the maximum axial compressive displacement before the beam bottom flange contacts the column flange. The equations derived by Sarraj (2007) are adopted in this component-based model to represent the fin-plate in bearing, beam web in bearing and bolt in shear. The equations developed by Block (2006) are used to calculate the force-displacement curves of the column web in compression. The

simplified ‘plastic cone’ model developed by Dong (2016) is used to calculate the maximum strength of the bolt pull-out component. As for the face-plate-semi-cylindrical component, the analytical models based on simple plastic theory, developed by the authors (Liu et al., 2020a) are used to generate its characteristics.

Block (2006) and Dong (2015) adopted the classic Masing rule (Gerstle, 1988) to represent the irreversible deformation of a component when the deformation of this component enters the plastic range. However, since the tensile and compressive force-displacement relationships of the face-plate-semi-cylindrical component are not identical in shape (Liu et al., 2020a), the Masing rule is not applicable to this connection. Therefore, it is assumed that the unloading path of the connection is linear and its slope is equal to that of the initial linear-elastic part of the loading curve, as shown in Figure 4 (a). In order to simulate the temperature-dependent characteristics of the force-displacement relationships of the components in fire, the ‘Reference Point’ concept is introduced to generate the unloading curve of each component at changing temperatures. As shown in Figure 4 (a), all force-displacement curves of a component at different temperatures unload to the same Reference Point. The complete force-displacement relationship of a spring row under a complete axial load cycle of the component-based model for the bare-steel connection is shown in Figure 4 (b). The blue loop starts in pulling, and then the spring row is unloaded and pushed back to its original state. The red loop starts in pushing, and the spring row is then unloaded and pulled back to its original shape. Figure 4 (b) shows that the unloading stiffness is very large, resulting in a sudden change of spring row force when unloading occurs.

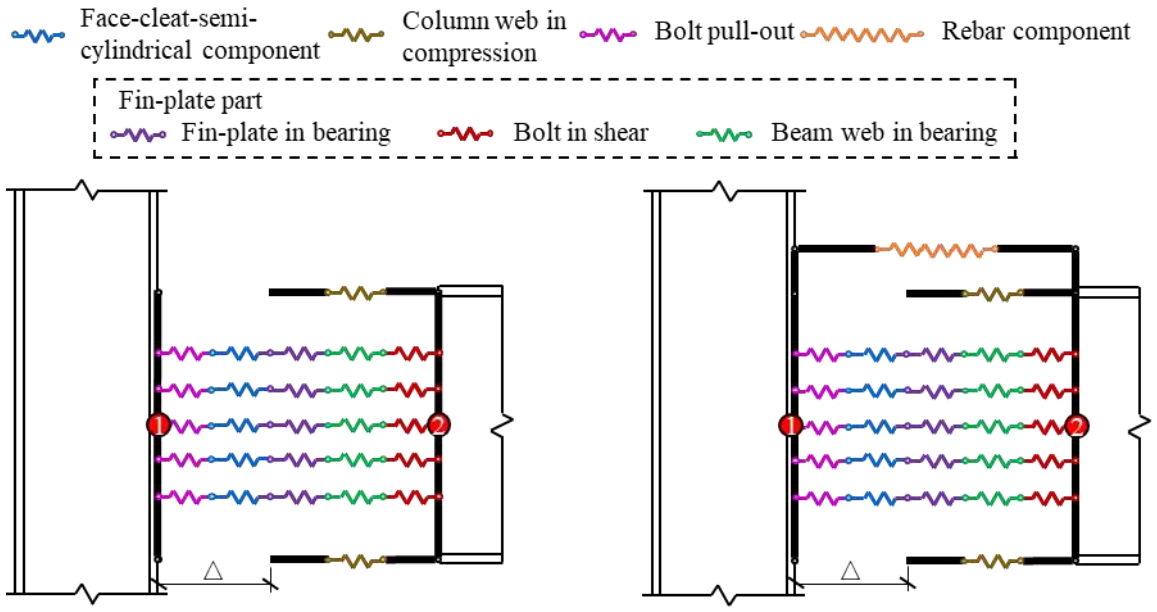

(a) Component-based model of bare-steel connection (b) Component-based model of composite connection

Figure 3. Component-based models of the ductile connection

The composite connection model is established by adding a rebar component to the bare-steel connection model (Liu et al., 2021a), as shown in Figure 3 (b). Concrete in tension is ignored since the connection is within the hogging moment zone and the tensile strength of concrete is negligible. The rebar component, developed by the authors (Liu et al., 2021a) on the basis of the simple rebar slip model proposed by Sezen and Setzler (2008), can consider the pull-out of reinforcing bars and the influence of weld points in the mesh. It should be emphasized here that the composite frames used in this paper are typical composite designs for fire with light reinforcement, and the calculation of the development length of the rebar adjacent to the crack in the rebar component takes into account the contribution of the weld points on the transverse reinforcing bars in the mesh. Considering different combinations of development length, rebar stress and weld strength, there are different situations for plain rebars and deformed rebars, all of which can be considered in the rebar component. According to the experimental results obtained by Al-Jabri (1999), it is further assumed that a discrete concrete crack occurs at the outer surface of the column flange. The development length of the rebar on one side of the concrete crack is limited by the first three weld points, whereas the development length on the other side is limited by the first weld point and the centre line of column section. Once the slips of the rebar on both sides of the concrete crack are obtained, the crack-width

or the total displacement of the rebar component is the sum of the slips on both sides.

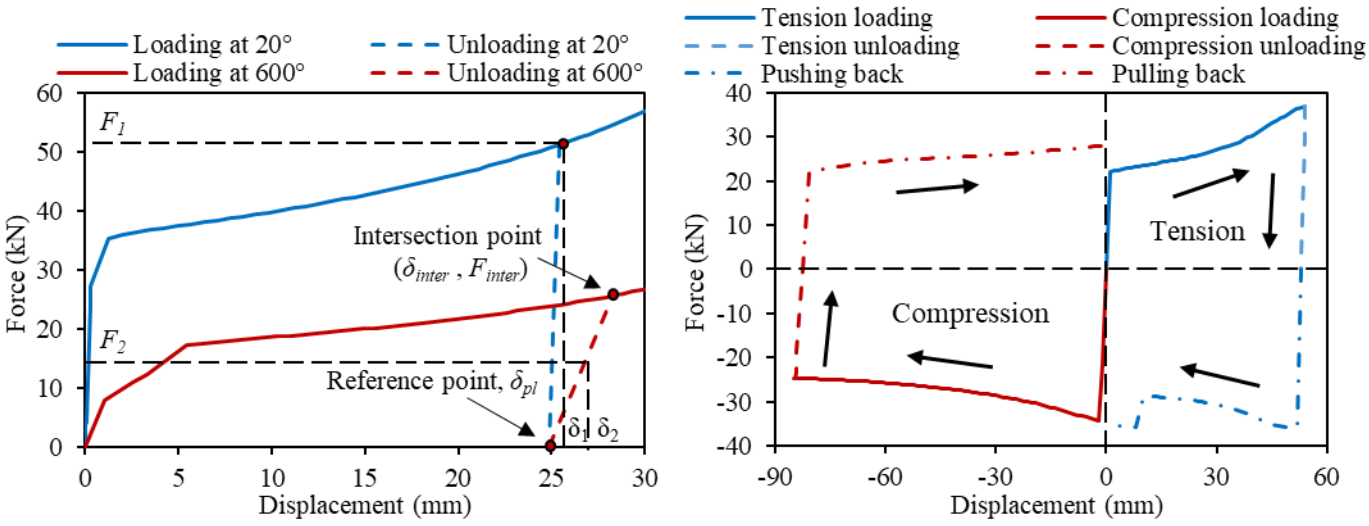

(a) Unloading with changing temperatures

(b) Loading and unloading process of a spring row

Figure 4. Illustrations of the unloading of a component and the loading-unloading force-displacement curve of a spring row

4 VALIDATION OF COMPONENT-BASED MODELS

4.1 Validation of the component-based model against experiments

In this section, the experiments conducted by Kalawadwala (2018) are used to test the component-based model at ambient temperature, and the experiments by Briggs (2016) are used to validate the component-based model at elevated temperatures. The dimensions of Kalawadwala's specimens are documented in a previous paper (Liu et al., 2019b), and are not repeated here. Kalawadwala carried out three experiments, where the deformed shapes of three specimens are similar, as shown in Figure 5. Figure 5 (a) illustrates the initial state of the specimen and Figure 5 (b) shows the deformed shape of the specimen under pushing. Figure 5 (c) shows that the specimen is pulled back to its original state, and Figure 5 (d) shows the specimen when it is eventually stretched flat. The comparison of results between the three experiments and the component-based model are shown in Figure 6. In general, the results from the component-based model are in good agreement with the experimental results at ambient temperature. Figure 6 shows that the slopes of the initial linear elastic loading path and that of the unloading path given by the experiments are lower than those given by the component-based models. This may be due to the slip between the clamps of the

testing machine and the specimen. The slopes of the experimental unloading curves are lower than those of the unloading curves calculated using the component-based models, indicating that a softer unloading path is needed to further improve the component-based models. It should also be noted that the softer unloading path will affect the location of the 'reference point'

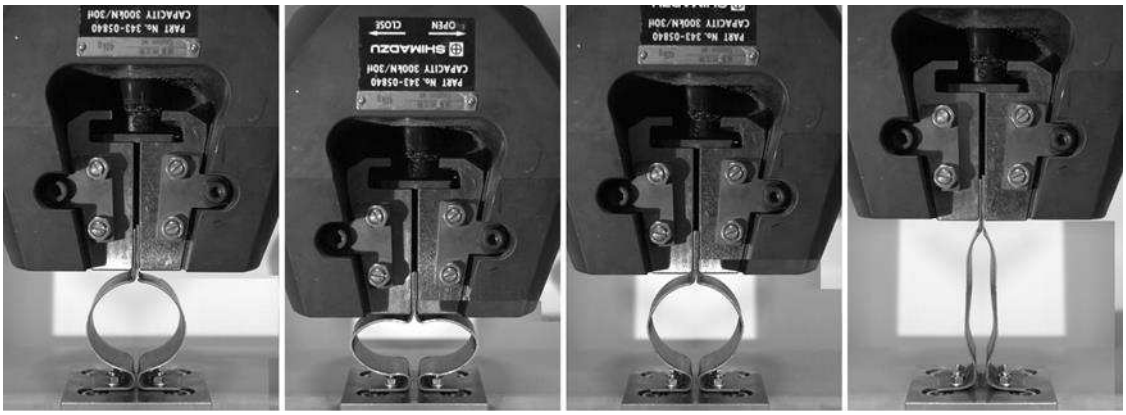

(a) Initial state (b) Pushing (c) Pulling back (d) Pulling

Figure 5. Deformation of the connection specimen during ambient-temperature experiment 1

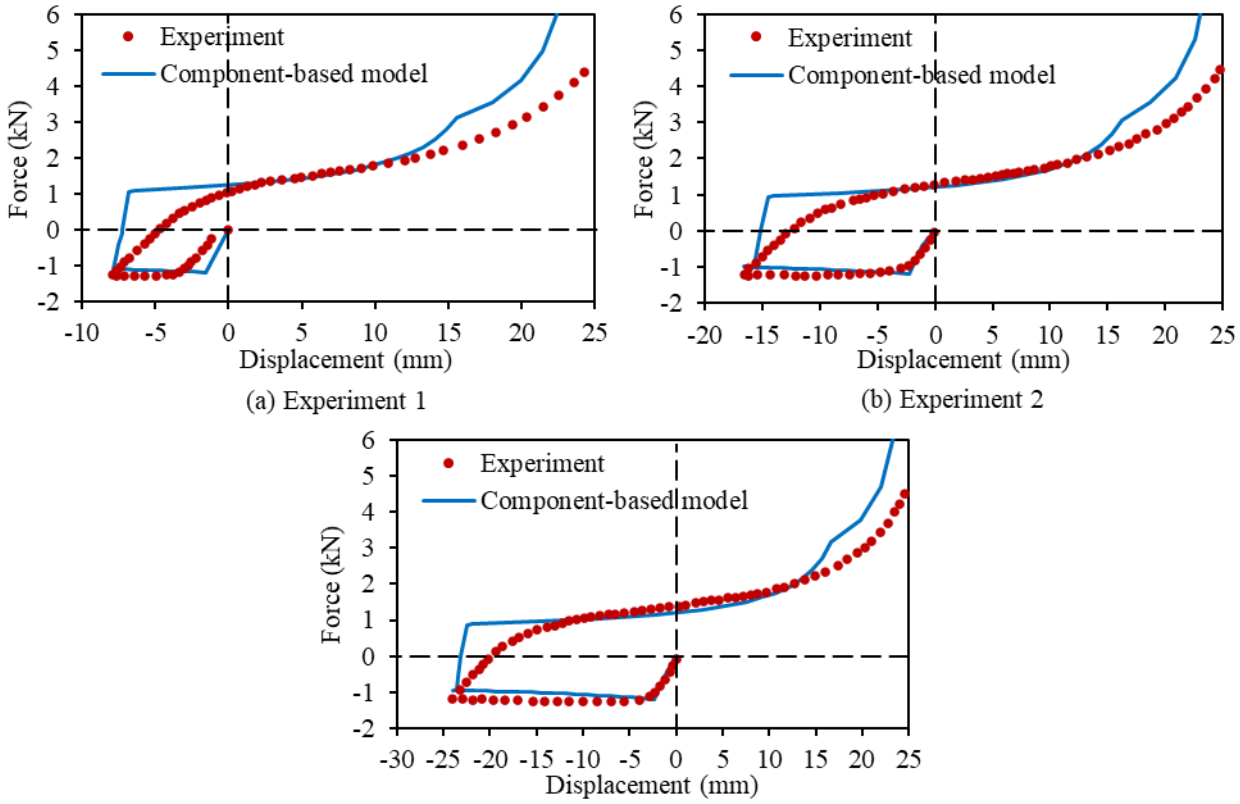

(a) Experiment 1 (b) Experiment 2

(c) Experiment 3

Figure 6. Comparison of component-based model against experiments at ambient temperature

The 3D printing technique was used by Briggs to produce 316L Austenitic stainless-steel specimens. Four temperatures, 350°C, 450°C, 550°C and 650°C, were selected to carry out elevated-temperature compression tests. As shown in Figure 7, the force-displacement curves at all temperatures follow the same general trend, indicating a slight decrease of compressive force as the compressive displacement increases. The discrepancy between the component-based model and experimental results shown in Figure 7 may be caused by the uncertainty in the material properties of 316L stainless steel. The yield and ultimate strengths obtained from Briggs' coupon tests are used in the component-based model. However, due to the limitations of the test equipment, Briggs did not anneal his specimens to relieve residual stress in the coupon tests. Herliansyah (2015) studied the effect of annealing temperature on 316L stainless steel, and found that annealing can significantly reduce the yield and ultimate strengths, whilst increasing the ductility of the 316L steel. In addition, Briggs did not specifically measure Young's modulus in his material tests, and so the value obtained by Wilkinson (2015) is adopted in the component-based model calculation, which might also cause the discrepancy. The large increase in compression force, beyond -8mm displacement, of the experimental results indicates the contact between the semi-cylindrical section and face-plate at large compressive displacement. The compression force of the connection under any given displacement should decrease with the increase of temperature. In general, the experiments at high temperatures show that temperature only affects material properties and does not affect the deformation mode of the connection.

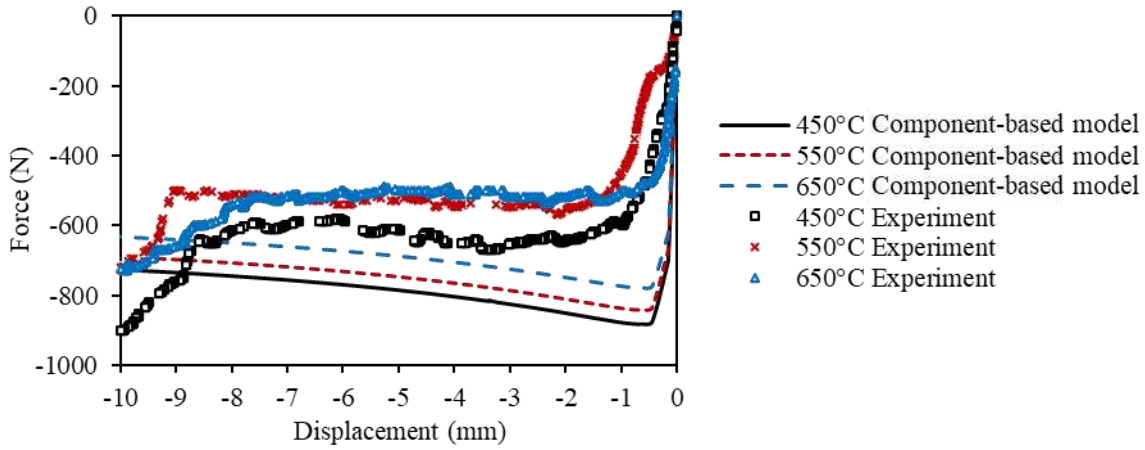

Figure 7. Comparison of component-based model against experiments at elevated temperatures

4.2 Validation of the bare-steel connection element against Abaqus simulations

The component-based model of the bare-steel ductile connection has been converted into a two-noded connection element following the principles of the finite element method, and has been incorporated into the software Vulcan (Liu et al., 2020c). In order to verify whether the bare-steel connection element has been correctly incorporated into Vulcan, a 2-D bare-steel sub-frame model shown in Figure 8 (a) is built using both Vulcan and Abaqus. A UDL of 42.64 kN/m is applied on the beam generating a load ratio of 0.4 with respect to simply supported beam. To save computational cost, only half of the model is built, and symmetric boundary conditions are applied at the mid-span of the beam. It is assumed that the lower floor column and the connection are protected to the same level, and their temperatures are half of the beam temperature, whereas the upper-storey column remains unheated. Table 1 shows the detailed dimensions of the ductile connection used in the sub-frame model. In reality, connections tend to experience much lower temperatures than the adjacent structural members due to their high massivity. Lawson (1990a, 1990b) assumed that the temperature of the connection was about 70% of that of the beam bottom flange at the beam mid-span. In this sub-frame model, the standard fire curve is used, and it is assumed that the connection and the lower column are protected to the same level. Therefore, the temperatures of the connection and the lower column are set to be equal to half of the beam temperature.

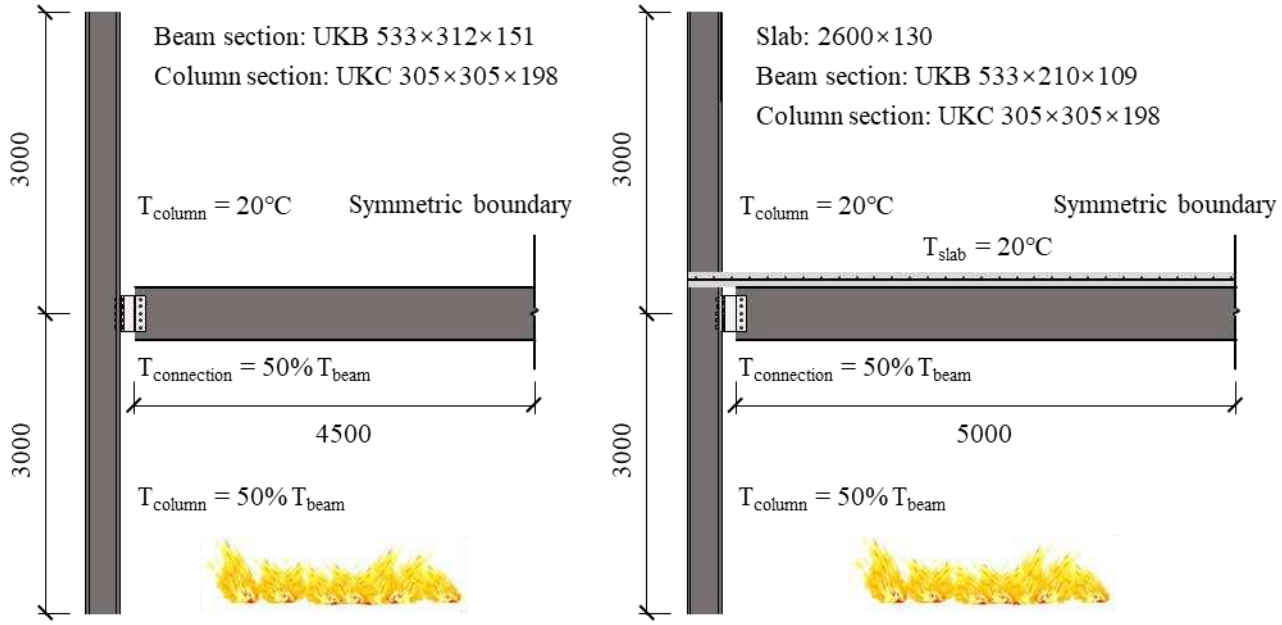

(a) 2-D bare-steel sub-frame model

(b) 2-D composite sub-frame model

Figure 8. 2-D sub-frame model (units in mm)

Table 1. Connection size

Inner radius of semi-cylindrical section (mm)	50
Plate thickness (mm)	6
Fin-plate width (mm) × depth (mm)	100×360
Face-plate width (mm) × depth (mm)	100×360
Number of bolt rows	5

The comparisons of results between Vulcan and Abaqus are shown in Figure 9 (a) and (b). It can be seen that the Vulcan results are in good agreement with the Abaqus results, confirming that the Vulcan component-based bare-steel connection element can simulate the connection behaviour as well as the detailed FE modelling. Figure 9 (c) and (d) show the force-temperature and displacement-temperature curves of each spring row of the connection element during the whole analysis. This figure shows that all the spring rows undergo compressive displacement due to the thermal expansion of the connected beam at the initial heating stage. The compressive displacement of each spring row begins to decrease at around 600°C, and eventually changes to tensile displacement when the connected beam enters the catenary action stage at about 660°C. After that, the tensile displacement of each spring row continues to increase until the limit is reached. Spring row 1 (the top spring row) experiences the largest tensile displacement and is the first row to fail due to the bolt pull-out at that level, compared with other spring rows. After the failure of Spring row 1, other spring rows fail row-by-row in the same manner. The connection will be considered as failed once all the spring rows have failed, and will be deleted from the model, leading to the detachment of the connected beam from the column.

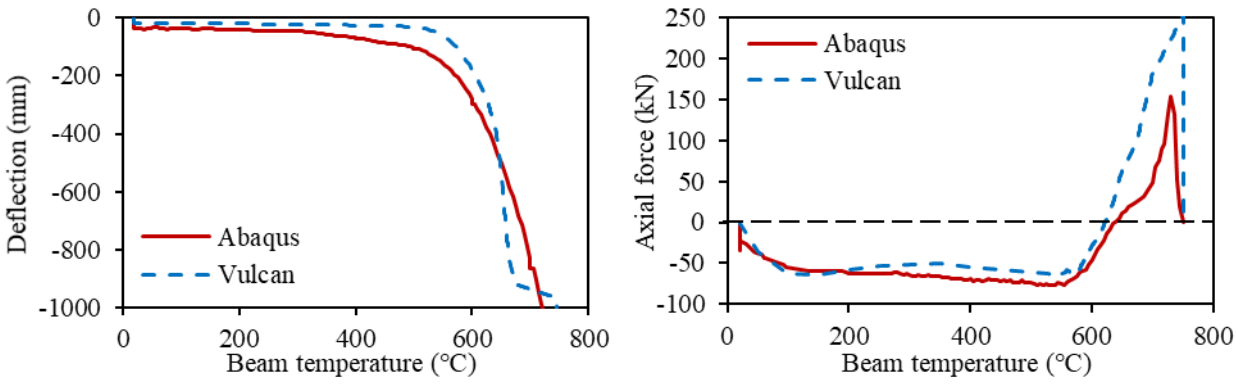

(a) Mid-span beam deflection

(b) Connection axial force

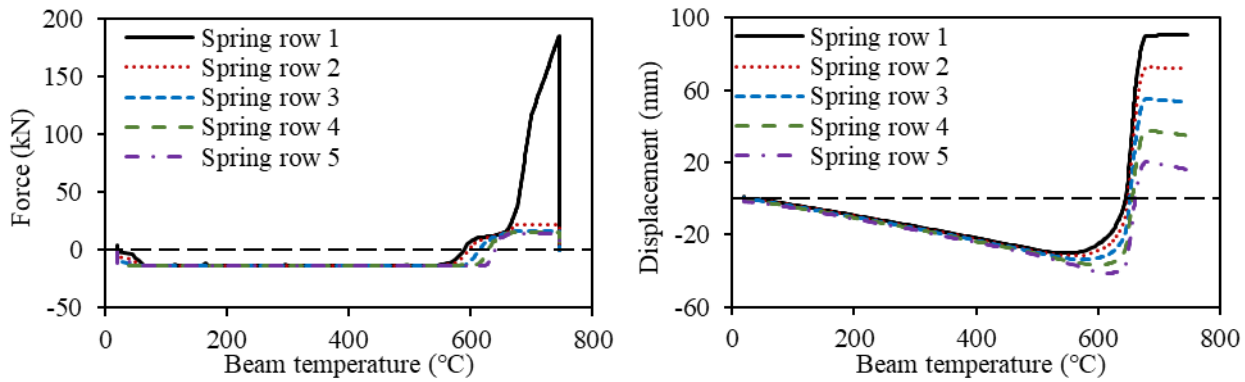

(c) Temperature-force curves

(d) Temperature-displacement curves

Figure 9. Results of the 2-D bare-steel sub-frame model

4.3 Validation of the composite connection element against Abaqus simulations

Following the same method as for the bare-steel connection model, the composite component-based connection model has also been converted into a connection element and incorporated into Vulcan (Liu et al., 2021a). In this section, the 2-D composite sub-frame shown in Figure 8 (b) is modelled using Vulcan and Abaqus to validate the composite connection element. The dimensions of the ductile connection in the composite frame are the same as those of the ductile connection used in the bare-steel frame, as listed in Table 1. Full shear connection is assumed between the slab and the beam, and is achieved by shared nodes between the slab elements and the beam elements in the Vulcan model. In the Abaqus model, shear studs are not modelled in detail, and full shear connection is achieved by fully tying the bottom of the slab and the top flange of the steel beam. It should be noted that the width of the concrete slab used here is the effective width of the concrete flange of the composite beam, which is $b_{eff} = l/4 + b_0$, where b_0 represents the width of the steel flange occupied by shear studs. A comparison of results between Vulcan and Abaqus is shown in Figure 10, and the evolution over time of force and displacement of each spring row of the composite connection element are shown in Figure 11.

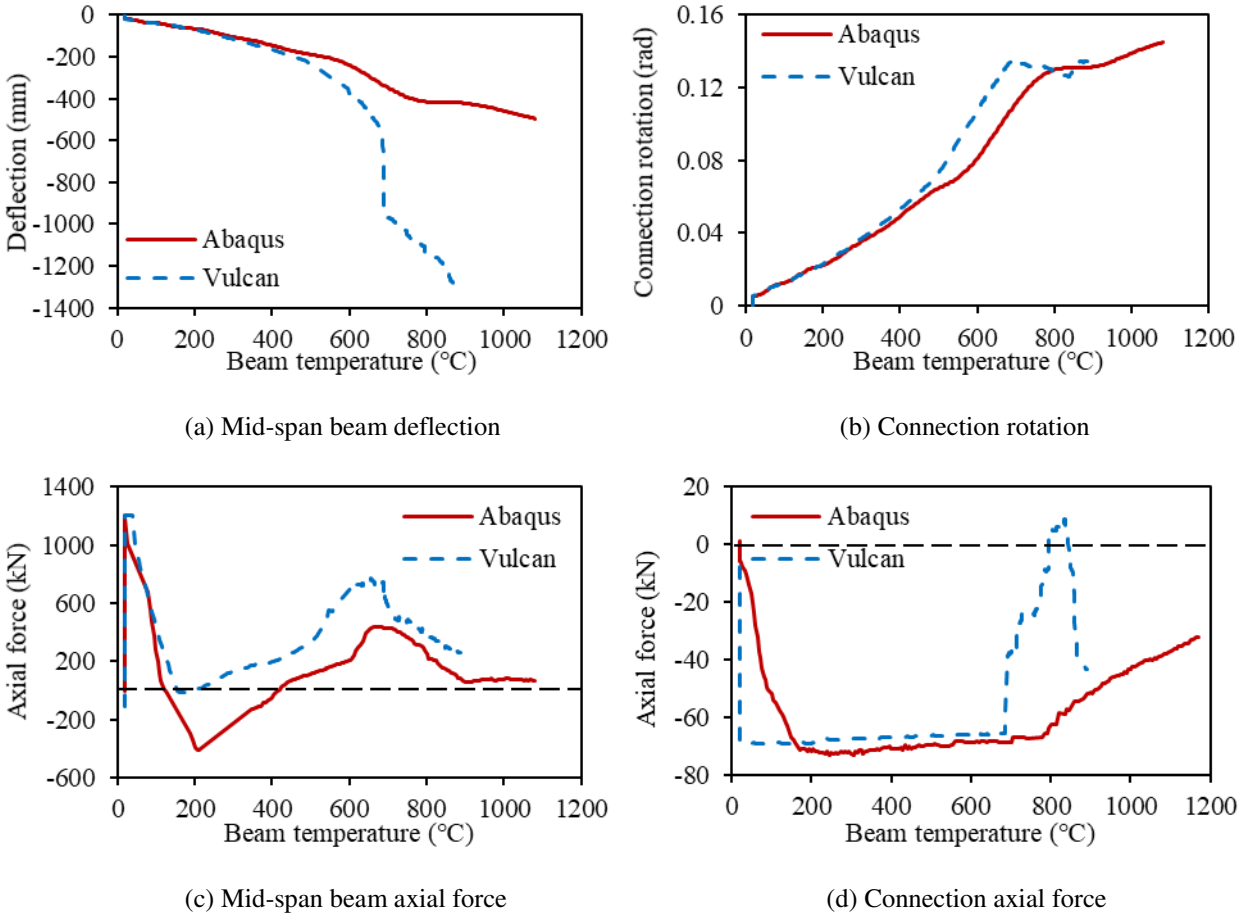

(a) Mid-span beam deflection

(b) Connection rotation

(c) Mid-span beam axial force

(d) Connection axial force

Figure 10. Results of the 2-D composite sub-frame model

The discrepancies between the Vulcan and Abaqus results arise because the approaches that these two softwares use to simulate the connection are fundamentally different:

1. In the Vulcan model, it is assumed that a discrete concrete crack is formed at the outer surface of the column flange, which is difficult to achieve in the Abaqus model since the 'concrete damage plasticity' function can only consider smeared continuous concrete cracking, which does not represent a localized crack in detail. This makes the composite slab of the Abaqus model stronger than that of the Vulcan model.

2. As mentioned in Section 3, since the stiffness of the unloading curve is very large, the spring row force changes its sense very suddenly when unloading occurs (Figure 4 (b)). This elastic unloading property is not considered in the Abaqus model.

Figure 10 (a) and (b) shows that the beam mid-span deflection and connection rotation given by the Vulcan model are larger than those of the Abaqus model, which can be explained by the first point above. There is

a sudden increase in the beam deflection of the Vulcan model at 686 ℃, which is due to the displacement reversal of the spring rows, as shown in Figure 11 (b). Figure 10 (c) shows a comparison between the mid-span beam axial forces of the Vulcan and Abaqus models. During the early heating stage, the initial tensile beam axial force decreases rapidly as temperature rises, due to the beam thermal expansion. Compared with the Vulcan model, the composite slab of the Abaqus model provides a stronger constraint to the thermal expansion of the beam, and so the beam axial force given by the Abaqus model decreases faster than that of the Vulcan model. The beam axial force begins to increase after around 200℃ due to the influence of thermal bowing, and decreases again at around 700℃ when the steel material loses most of its strength. Figure 10 (d) illustrates the comparison of the connection axial forces obtained from the Abaqus and Vulcan models. This figure shows that there is a sudden drop of the compressive connection axial force given by the Vulcan model at 686℃. After that, the connection axial force of the Vulcan model temporarily changes into tension at about 800 ℃, and then becomes compressive again. This reversal of the connection axial force can be explained by the second point above. Figure 11 (a) shows a sudden decrease of the compressive forces of all the spring rows at 686 ℃, which is caused by the changes of the displacement direction of all the spring rows shown in Figure 11 (b). This is manifested in the sudden decrease of the Vulcan connection compressive axial force (Figure 10 (d)) as mentioned above. When the beam temperature reaches 838 ℃, the displacements of all the spring rows change their direction again, leading to the reversal of the spring row force to compression. Accordingly, the Vulcan connection axial force becomes compressive again as shown in Figure 10 (d). It should be noted that such elastic unloading properties are not taken into consideration in the Abaqus model, which may explain the discrepancies between the Vulcan and Abaqus results shown in Figure 10 (a) and (d). In general, the Vulcan results correlate well with the Abaqus results, indicating that the composite connection element can be used to simulate the responses of composite structures with ductile connections to fire.

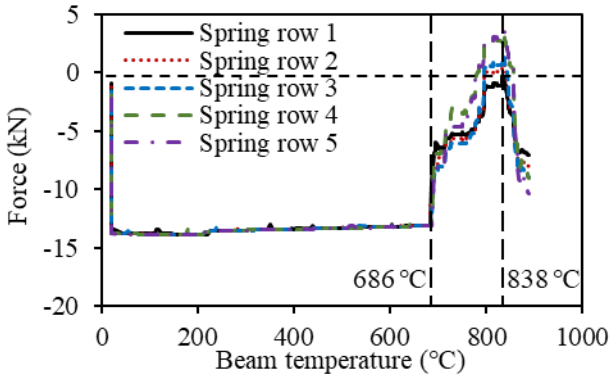

(a) Temperature-force curve of each spring row

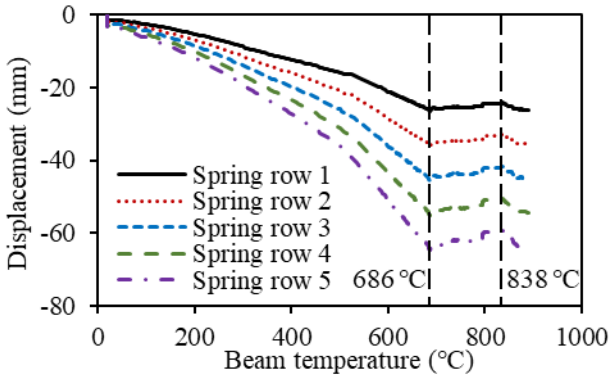

(b) Temperature-displacement curve of each spring row

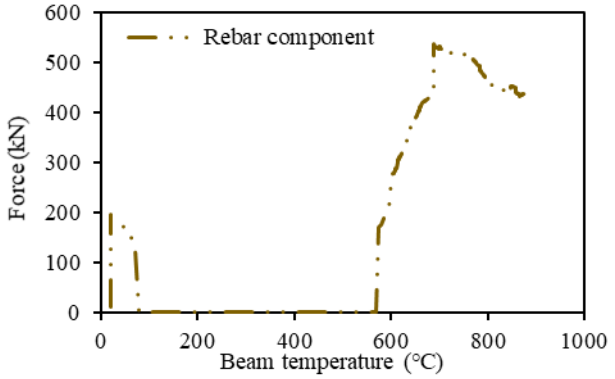

(c) Temperature-force curve of rebar component

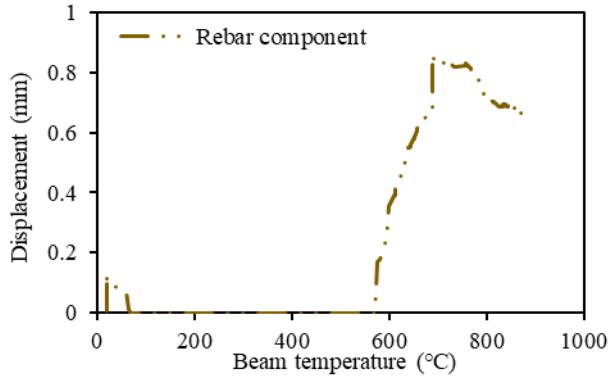

(d) Temperature-displacement curve of rebar component

Figure 11. Temperature-force and temperature-displacement curves of each spring row and rebar component

5 COMPARISON OF THE DUCTILE CONNECTION WITH OTHER CONNECTION TYPES

5.1 Performance comparison within bare-steel frames

In this section, the 2-D bare-steel sub-frame models shown in Figure 8 (a) with different connection types, including the ductile connection and idealised rigid and pinned connections, are created using Vulcan to compare their performances. Figure 12 shows the comparison of results, indicating that below about 600 °C, the mid-span deflection of the beam with ductile connection is lower than those of the beams with idealised connections. Beyond that temperature, the deflection of the beam with ductile connections increases rapidly, and finally exceeds those of the beams with idealised connections. Compared with the other connection types, the axial force generated in the ductile connection is significantly reduced, as shown in Figure 12 (b). This indicates that the ductile connection can provide additional axial and rotational ductility to accommodate both the thermal expansion of the connected beam during the initial heating stage and the net

contraction of connected beam when the beam enters the catenary action stage. The ductile connection can also contribute to the reduction of the axial forces, to which the surrounding structural members are subjected.

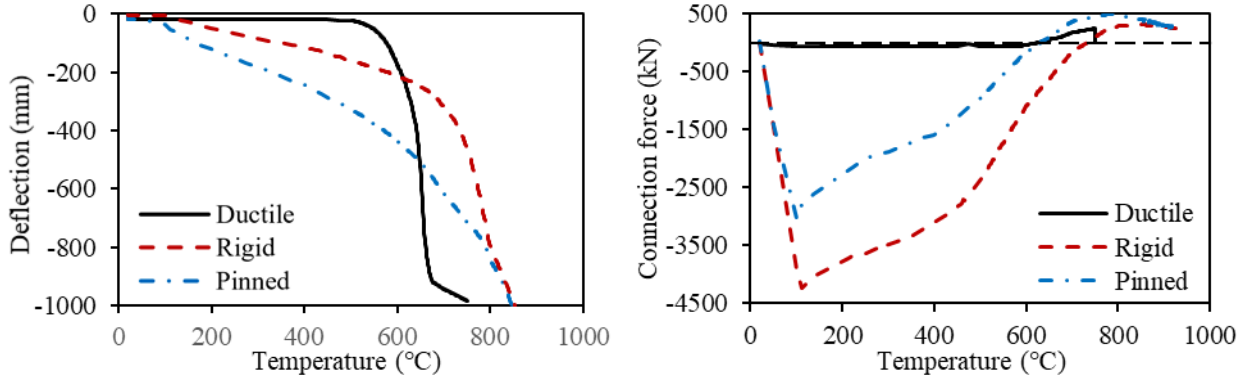

(a) Mid-span beam deflection

(b) Connection axial force

Figure 12. Performance comparison within bare-steel frame

5.2 Performance comparison within composite frame

The structural behaviour of connections within composite structures is quite different from that of connections within bare-steel frames, due to the existence and continuity of the composite slab. In addition, structural members within a composite frame always interact with each other and work as a whole. The influence of out-of-plane structural elements, particularly slabs, on the connection performance should be taken into consideration when modelling connections within composite structures. Therefore, in order to be as close to reality as possible, 3-D composite frame models with various connection types are built using Vulcan in this section, as shown in Figure 13 (a). The design of the composite frame, as shown in Figure 13 (a), is based on the typical frame used in the Cardington fire tests (Lennon et al., 1999, Wald et al., 2004). The dimensions of the ductile connection used in this composite frame are shown in Figure 13 (b). The permanent load and the imposed load are taken as 3.65 kN/m^2 and 3.5 kN/m^2 respectively, and the combined load applied on the slab in the fire limit state should be 3.65+3.5×0.5=5.4 kN/m^2. It is assumed that fire occurs on the lower floor and the standard fire curve is used; only the central secondary beam is unprotected, and its temperature is equal to the fire temperature. All the edge secondary beams, the primary

beams and the lower columns are protected to the same level, and their temperatures are set to be 70% of the fire temperature. The connection is assumed to be at the same temperature as the connected beam. Full shear connection is assumed between the beams and slab. The three connection types (ductile connection, idealised rigid and idealised pinned) adopted in Section 5.1, are again used in the 3-D composite frame models here.

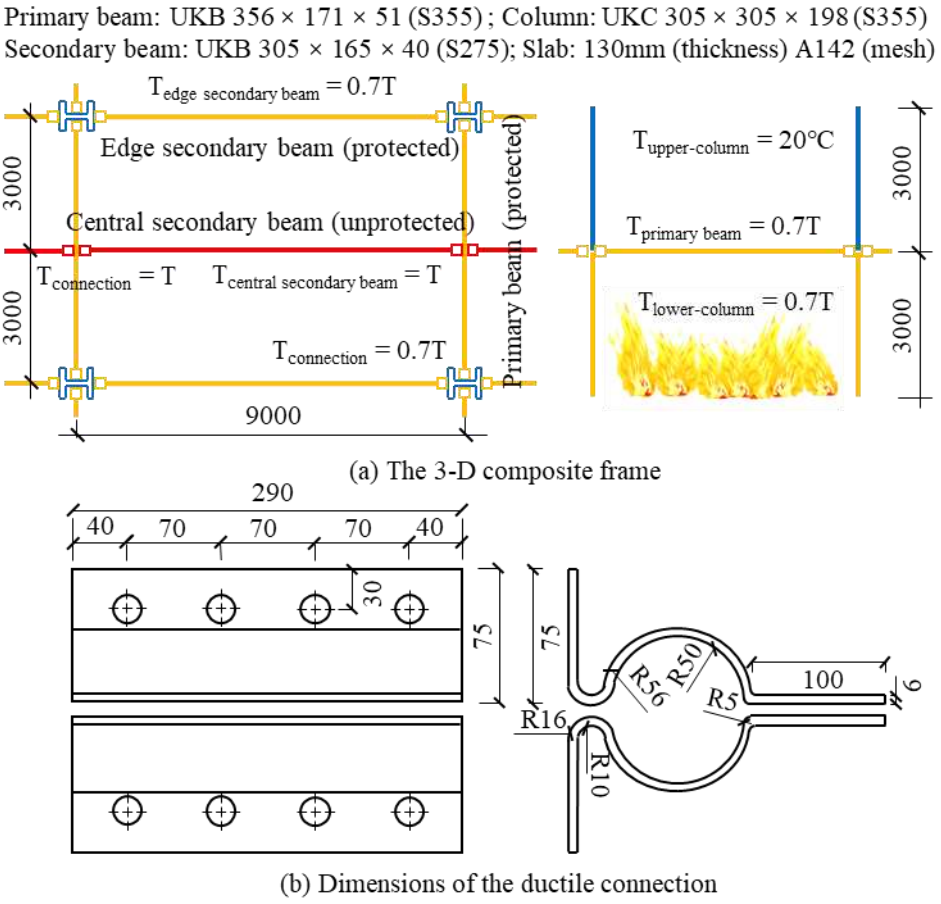

Figure 13. The 3-D composite frame model

The comparative results are shown in Figure 14. Figure 14 (a) – (c) show that the deflection of the beam with ductile connection is very close to that of the beam with pinned connection, and they are all larger than the deflection of the beam with rigid connections, indicating the ductile and pinned connections apply less restraints on to the beam, compared with the rigid connections. Figure 14 (d) – (f) show that the axial force generated in the ductile connection is significantly reduced compared with the rigid and pinned connections. These comparative results confirm that the ductile connection can also provide excellent axial

and rotational deformability in composite construction.

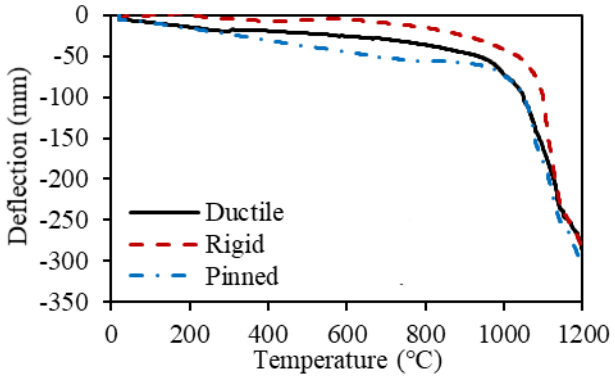

(a) Mid-span deflection of primary beam

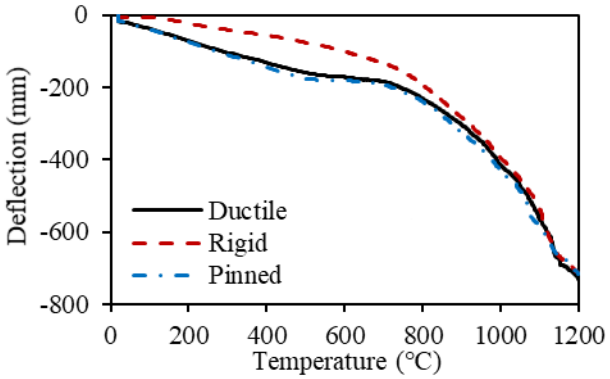

(b) Mid-span deflection of central secondary beam

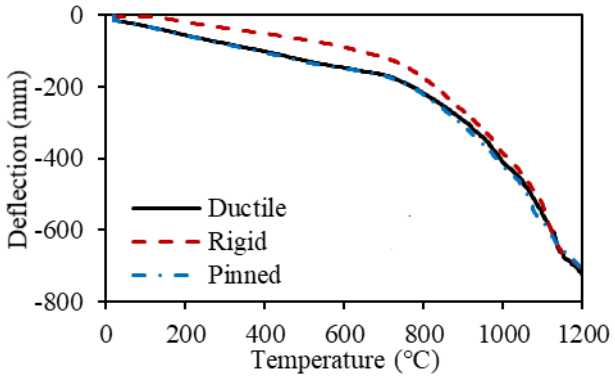

(c) Mid-span deflection of edge secondary beam

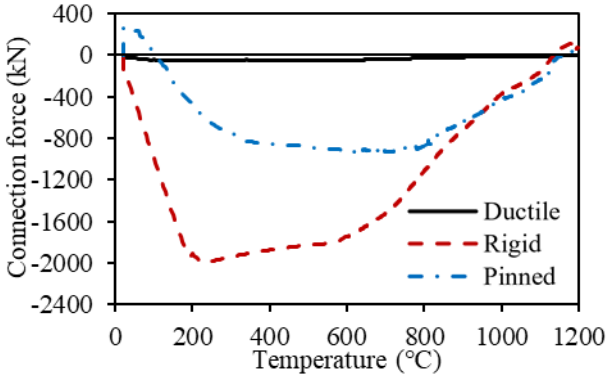

(d) Primary beam to column connection

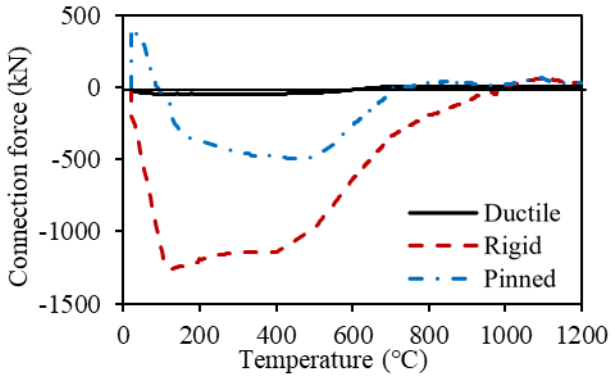

(e) Central secondary beam to primary beam connection

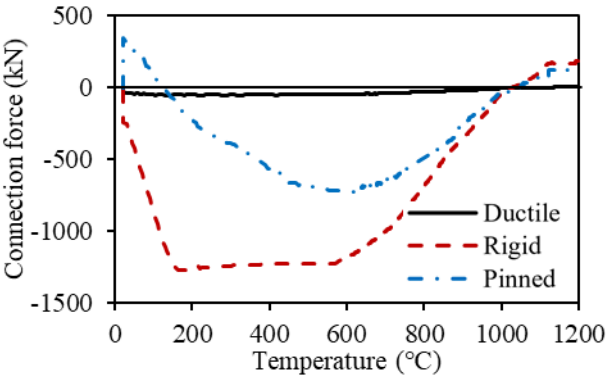

(f) Edge secondary beam to column connection

Figure 14. Comparison results (central secondary beam temperature)

6 CONCLUSIONS

Connections play a key role in the survival or collapse of structures under fire conditions. In order to

improve the ductility of connections and to enhance the robustness of structures in fire, a novel connection with axial and rotational ductility has been proposed by the authors. In this paper, the ductility demands of bare-steel and composite beams in fire, the design of the ductile connection, and the component-based models of the bare-steel and composite ductile connections have been presented.

The component-based model of the bare-steel ductile connection has been validated against experiments at both ambient and elevated temperatures. Results obtained using the component-based model correlate well with the experimental results at ambient temperature. At elevated temperatures, the results from the component-based model and experiments do not match as well as at ambient temperature; the uncertainty in the material properties might be responsible for this. A 2-D bare-steel sub-frame with ductile connections was modelled using Vulcan and Abaqus. The Vulcan results are in good agreement with the Abaqus results, indicating that the bare-steel connection element has been correctly incorporated into Vulcan. Through the analysis of the Vulcan model results, it is found that the top spring row experiences the largest tensile displacement and is the first to fail by bolt pull-out. After this, other spring rows fail row-by-row in the same manner. It should be noted that the unloading path used in the component-based models is simplified as linear, and its stiffness is set to be equal to the initial elastic loading stiffness. In this way, the unloading stiffness is quite large, resulting in a sudden change of the spring row force when unloading occurs. This can lead to the slight oscillation mode of Vulcan results, especially manifested in the result curves involving forces. A softer unloading path is certainly needed to improve the component-based model in the future work.

A 2-D composite sub-frame was used to check the performance of the composite ductile connection element, comparing the results from Vulcan and Abaqus models. Comparison of the results shows that the Vulcan model is in good agreement with the detailed Abaqus model, until the axial displacements of the connection components change direction. In the proposed connection element, the displacement reversal of a spring row leads to a rapid change in the spring row force. This characteristic is not taken into consideration in the Abaqus model. The current indication is that the Vulcan composite connection element can be used to facilitate global frame analysis to investigate the effect of adopting the ductile connection in composite

structures under fire conditions.

The performance of the ductile connection within 2-D bare-steel and 3-D composite frames has been compared with that of idealized connection types, both pinned and rigid. Results show that the connection force can be significantly reduced when using the ductile connection in both bare steel and composite frames. This indicates that the proposed ductile connection can provide excellent axial and rotational deformabilities to accommodate the deformation of connected beams in fire, thus potentially preventing the fracture of connections and enhancing the fire robustness of structures.

REFERENCES

AL-JABRI, K. S. 1999. *The behaviour of steel and composite beam-to-column connections in fire.* University of Sheffield.

BLOCK, F. M. 2006. *Development of a component-based finite element for steel beam-to-column connections at elevated temperatures.* University of Sheffield Sheffield, UK.

BRIGGS, J. 2016. Experimental investigation of the performance of a modified 3D printed 316L stainless steel structural connection at elevated temperatures.

CAI, J., BURGESS, I. & PLANK, R. 2003. A generalised steel/reinforced concrete beam-column element model for fire conditions. *Engineering Structures,* 25**,** 817-833.

CEN 2005. Eurocode 3: Design of steel structures—Part 1-8: Design of joints.

DONG, G. 2016. *Development of a General-Purpose Component-based Connection Element for Structural Fire Analysis.* University of Sheffield.

DONG, G., BURGESS, I., DAVISON, B. & SUN, R. 2015. Development of a general component-based connection element for structural fire engineering analysis. *Journal of Structural Fire Engineering,* 6**,** 247-254.

FISCHER, E. C. & VARMA, A. H. 2017. Fire resilience of composite beams with simple connections: Parametric studies and design. *Journal of Constructional Steel Research,* 128**,** 119-135.

GERSTLE, K. H. 1988. Effect of connections on frames. *Journal of Constructional Steel Research,* 10**,** 241-267.

HERLIANSYAH, M. K., DEWO, P., SOESATYO, M. H. & SISWOMIHARDJO, W. The effect of annealing temperature on the physical and mechanical properties of stainless steel 316L for stent application.

Instrumentation, Communications, Information Technology, and Biomedical Engineering (ICICI-BME), 2015 4th International Conference on, 2015. IEEE, 22-26.

HU, Y., DAVISON, B., BURGESS, I. & PLANK, R. 2009. Component modelling of flexible end-plate connections in fire. *International Journal of Steel Structures,* 9**,** 1-15.

HUANG, Z., BURGESS, I., PLANK, R., VULCAN, REISSNER, M. & BRE 1999. THREE-DIMENSIONAL MODELLING OF TWO FULL-SCALE, FIRE TESTS ON A COMPOSITE BUILDING. *Proceedings of the Institution of Civil Engineers-Structures and Buildings,* 134**,** 243-255.

HUANG, Z., BURGESS, I. W. & PLANK, R. J. 2003a. Modeling membrane action of concrete slabs in composite buildings in fire. I: Theoretical development. *Journal of structural engineering,* 129**,** 1093-1102.

HUANG, Z., BURGESS, I. W. & PLANK, R. J. 2003b. Modeling membrane action of concrete slabs in composite buildings in fire. II: Validations. *Journal of Structural Engineering,* 129**,** 1103-1112.

HUANG, Z., BURGESS, I. W. & PLANK, R. J. 2009. Three-dimensional analysis of reinforced concrete beam-column structures in fire. *Journal of structural engineering,* 135**,** 1201-1212.

KALAWADWALA, S. 2018. Investigation of the performance of innovative connection under hazard loading.

LAWSON, R. 1990a. Behaviour of steel beam-to-column connections in fire. *Structural engineer,* 68**,** 263-71.

LAWSON, R. 1990b. *Enhancement of fire resistance of beams by beam to column connections*, Steel Construction Institute UK.

LENNON, T. & MOORE, D. 2003. The natural fire safety concept—full-scale tests at Cardington. *Fire Safety Journal,* 38**,** 623-643.

LENNON, T., MOORE, D. & BAILEY, C. 1999. The behaviour of full-scale steel-framed buildings subjected to compartment fires. *The Structural Engineer,* 77**,** 15-21.

LESTON-JONES, L. C. 1997. *The influence of semi-rigid connections on the performance of steel framed structures in fire.* University of Sheffield.

LI, J.-T., LI, G.-Q., LOU, G.-B. & CHEN, L.-Z. 2012. Experimental investigation on flush end-plate bolted composite connection in fire. *Journal of Constructional Steel Research,* 76**,** 121-132.

LIU, Y., HUANG, S.-S. & BURGESS, I. Ductile connections to improve structural robustness in fire. Proceedings of the 6th Applications of Structural Fire Engineering Conference (ASFE'19), 2019a Singapore. Nanyang University of Technology

LIU, Y., HUANG, S.-S. & BURGESS, I. 2019b. Investigation of a steel connection to accommodate ductility demand of beams in fire. *Journal of Constructional Steel Research,* 157**,** 182-197.

LIU, Y., HUANG, S.-S. & BURGESS, I. 2020a. Component-based modelling of a novel ductile steel connection. *Engineering Structures,* 208**,** 110320.

LIU, Y., HUANG, S.-S. & BURGESS, I. Investigation of the performance of a novel ductile connection within bare-steel and composite frames in fire. Proceedings of the 11th International Conference on Structures in Fire (SiF2020), 2020b Asutralia, Queensland. The University of Queensland, 662-672.

LIU, Y., HUANG, S.-S. & BURGESS, I. 2020c. Performance of a novel ductile connection in steel-framed structures under fire conditions. *Journal of Constructional Steel Research,* 169**,** 106034.

LIU, Y., HUANG, S.-S. & BURGESS, I. 2021a. Fire performance of axially ductile connections in composite construction. *Fire Safety Journal***,** 103311.

LIU, Y., HUANG, S.-S. & BURGESS, I. Performance of ductile connections in 3-D composite frames under fire conditions. Applications of Structural Fire Engineering, Proceedings, 2021b. University of Ljubljana, 43-48.

LIU, Y., HUANG, S. S. & BURGESS, I. 2021c. A numerical study on the structural performance of a ductile connection under fire conditions. *ce/papers,* 4**,** 1196-1202.

MCALLISTER, T. & CORLEY, G. 2002. *World Trade Center Building performance study: Data collection, preliminary observations, and recommendations*, Federal Emergency Management Agency.

NAJJAR, S. & BURGESS, I. 1996. A nonlinear analysis for three-dimensional steel frames in fire conditions. *Engineering structures,* 18**,** 77-89.

SARRAJ, M. 2007. *The behaviour of steel fin plate connections in fire.* University of Sheffield.

SARRAJ, M., BURGESS, I., DAVISON, J. & PLANK, R. 2007. Finite element modelling of steel fin plate connections in fire. *Fire Safety Journal,* 42**,** 408-415.

SEZEN, H. & SETZLER, E. J. 2008. Reinforcement slip in reinforced concrete columns. *ACI Structural Journal,* 105**,** 280.

SPYROU, S. 2002. *Development of a component based model of steel beam-to-column joints at elevated temperatures.* University of Sheffield.

TAIB, M. & BURGESS, I. 2013. A component-based model for fin-plate connections in fire. *Journal of Structural Fire Engineering,* 4**,** 113-122.

WALD, F., SILVA, S., MOORE, D. & LENNON, T. Structural integrity fire test. Proceedings Nordic Steel Conference, 2004.

WILKINSON, H. 2015. Catastrophic Fire-Testing of 3D Printed Stainless Steel.

YU, H., BURGESS, I., DAVISON, J. & PLANK, R. 2009a. Development of a yield-line model for endplate connections in fire. *Journal of Constructional Steel Research,* 65**,** 1279-1289.

YU, H., BURGESS, I., DAVISON, J. & PLANK, R. 2009b. Tying capacity of web cleat connections in fire, Part 2: Development of component-based model. *Engineering structures,* 31**,** 697-708.